RSC Advances

PAPER

Cite this: *RSC Adv.*, 2016, **6**, 94287

Pressure-induced phase transitions of β-type pyrochlore $CsTaWO_6$†

F. X. Zhang,*[a] C. L. Tracy,[b] J. Shamblin,[c] R. I. Palomares,[c] M. Lang,[c] S. Park,[b] C. Park,[d] S. Tkachev[e] and R. C. Ewing[b]

Received 16th May 2016
Accepted 18th September 2016

DOI: 10.1039/c6ra11185h

www.rsc.org/advances

The β-type pyrochlore $CsTaWO_6$ was studied by synchrotron X-ray diffraction (XRD) and Raman scattering methods up to pressures of 43 GPa using a diamond anvil cell (DAC). With increasing pressure, the cubic pyrochlore in space group of $Fd\text{-}\bar{3}m$ transforms to an orthorhombic structure (space group: *Pnma*) at 5.9 GPa and then to a monoclinic structure (space group: $P2_1/c$) at ~18 GPa. The structural evolution in $CsTaWO_6$ is a continuous process and experimental results suggest that the initial cubic phase has a tetragonal distortion at ambient conditions. Both XRD and Raman measurements indicate that the pressure-induced phase transitions in $CsTaWO_6$ are reversible. These results may provide a structural explanation of previous experimental resistivity measurement results for the isostructural superconductor $K(Cs)Os_2O_6$ at high pressure conditions.

I. Introduction

Pyrochlore comprises a large family of oxides with more than 500 natural and synthetic chemical compositions.[1] Due to its structural and chemical flexibility, an increasing number of compounds with the pyrochlore structure are to be expected. The normal cubic pyrochlore structure has an ideal formula of $A_2B_2X_6Y$, where A and B are cations and X and Y are anions. The cubic pyrochlore (space group of $Fd\bar{3}m$) can be considered as a superlattice of the defect-fluorite structure but with 1/8 fewer anions. The A- and B-site cations occupy the 16d and 16c sites in the unit cell and the two independent anion sites are 48f for X and 8b for Y (Fig. 1a). The charge on the A- and B-site cations can be 3+/4+ or 2+/5+. Depending on the charge balance, many non-stoichiometric pyrochlores are possible. There are still unoccupied crystallographic sites (*e.g.*, 8a and 32e), that can be partially filled by both anions and cations in certain cases.[2,3] The structure of pyrochlore can be seen as two interpenetrating sublattices and the presence of defects on both the cation and anion sublattices is a unique characteristic of the pyrochlores. The B-site cations are each coordinated with six X anions in a corner-shared octahedral network which builds the main framework of the structure (Fig. 1a). For ideal stoichiometric pyrochlores, each Y anions is surrounded by four A-site cations in a corner-shared tetrahedral framework. Under extreme conditions, such as high temperature,[4] high pressure[5–9] or in a high energy radiation field,[10–13] the cation and anion sublattices may disorder or even become completely aperiodic, particularly when the A- and B-site cations have very different ionic radii. Because of the structural flexibility that is inherent to the pyrochlore structure, there are many technical applications: high anion conductive solid oxide fuel cells,[14,15] immobilization of radioactive nuclides[16–19] ion-exchange properties for the separation of radioactive nuclei.[20–24]

There is an additional type of pyrochlores which has alkaline metals in the cationic sublattice.[25,26] The octahedral framework in the lattice is similar to the structure of normal pyrochlores, but the composition is different. They have the same space group and the A-cations only occupy the 8b site instead of the 16d site in the channel (Fig. 1b), and the chemical composition is AB_2O_6. The β-type pyrochlore oxide structure has attracted

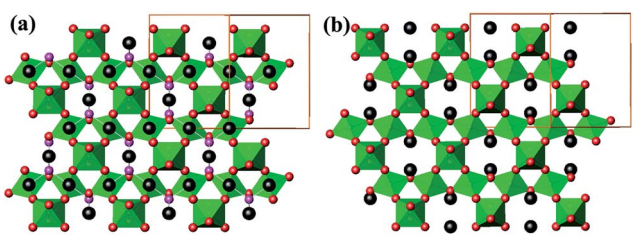

Fig. 1 Schematic crystal structure of (a) α-pyrochlore and (b) β-pyrochlore. Both α- and β-type pyrochlore have the cubic symmetry and there are tunnels projected along the [110] direction. The big cation in β-type pyrochlore occupies the 8a site which was anion site in α-type pyrochlore.

[a]*Department of Earth and Environmental Sciences, University of Michigan, Ann Arbor, MI 48109, USA. E-mail: zhangfx@umich.edu*

[b]*Department of Geological Sciences, Stanford University, Stanford, CA 94305, USA*

[c]*Department of Nuclear Engineering, University of Tennessee, Knoxville, TN 37996, USA*

[d]*HPCAT, Geophysical Laboratory, Carnegie Institution of Washington, Argonne, IL 60439, USA*

[e]*GSECARS, University of Chicago, IL 60439, USA*

† PACS numbers: 61.50.Ks, 61.10.Nz, 72.80.Ga.

great interests because of the discovery of Cu-free superconductors in alkaline metal osmium oxides. KOs_2O_6 has a superconducting transition temperature of 9.6 K,[27,28] and the same superconductivity was also found in oxides of $CsOs_2O_6$ (3.3 K)[29] and $RbOs_2O_6$ (6.3 K).[30] In addition, excellent dielectric and electrical conducting properties were found in some β-type pyrochlores, which has two different cations randomly distributed on the B-sites with combined charge configuration of $B^{5+}B^{6+}$ as that in CsNb(Ta)W(Mo)O_6.[31] Resistance measurements have revealed that the superconducting transition temperature of the β-type pyrochlore oxides has interesting pressure dependence, which first increases with pressure, but then drops at higher pressures.[32] In this paper, we investigated the structural changes of β-type pyrochlore $CsTaWO_6$ at high pressures by *in situ* XRD and Raman scattering measurements. The pressure-induced phase transformations are compared with those of regular pyrochlore oxides and used to provide a structural basis for understanding the changes in resistivity of alkaline superconductors with increasing pressure.

II. Experimental details

A polycrystalline sample of $CsTaWO_6$ was prepared by the solid-state reaction method using high purity Cs_2CO_3, Ta_2O_5 and WO_3 (all from Alfa Aesar with purity >99%). Stoichiometric ratios of the powders were thoroughly mixed in an agate motor with a methanol medium, and then uniaxially pressed into a pellet of a half-inch in diameter using a mechanical press. The pellet was heated at 1000 °C in air for 24 hours. The pellet was then ground into powder and pressed into a pellet again, and finally fired at 1100 °C for 24 hours. The structure of the sintered pellet was checked with a lab XRD diffractometer (Rigaku Miniflex) and the XRD profile confirmed the desired β-type pyrochlore phase. High pressure was generated using diamond anvil cells (DACs), and ruby chips or balls were used as the pressure marker.[33] A small quantity of powder was loaded into a 120 μm hole with a He gas pressure medium in a W gasket which was pre-indented to a thickness of ~40 μm. The *in situ* high pressure XRD measurements were performed at the 16 BMD beamline at the Advanced Photon Source, Argonne National Laboratory using a monochromatic 25 keV (wavelength 0.496 Å) X-ray beam. Debye rings were recorded with a CCD X-ray detector and then integrated into one-dimensional profiles using the Fit2d program.[34] All of the instrument parameters were calibrated using a CeO_2 standard. The collected XRD profiles were analyzed with the Rietveld refinement method using the software Fullprof.[35] For Raman measurement, two type IIa diamond anvils with ultralow fluorescence were used and a methanol/ethanol (4/1 volume) mixture served as the pressure transmitting medium. The Raman signal was activated with a 532 nm solid laser (Verdi 2) and collected with a high resolution liquid nitrogen cooled CCD detector (Symphony) attached to a modified SPEX-1250M spectrometer.

III. Results and discussion

XRD measurements indicate that the sample of $CsTaWO_6$ has a pure, single β-type pyrochlore structure. The selected XRD patterns at high pressure are shown in Fig. 2a. Phase transitions are observed from the splitting of Bragg peaks and the appearance of new diffraction peaks. In order to clearly distinguish the changes in Bragg diffraction maxima, the lower 2θ angle region is enlarged in Fig. 2b. In addition to the shift of Bragg peaks to larger 2θ angles due to the external pressure, some new diffraction peaks are clearly evident in the patterns starting at 8.3 GPa. The (111) peak at 2θ of 4.8° splits into two peaks at 12.4 GPa. This is indicative of symmetry loss in the

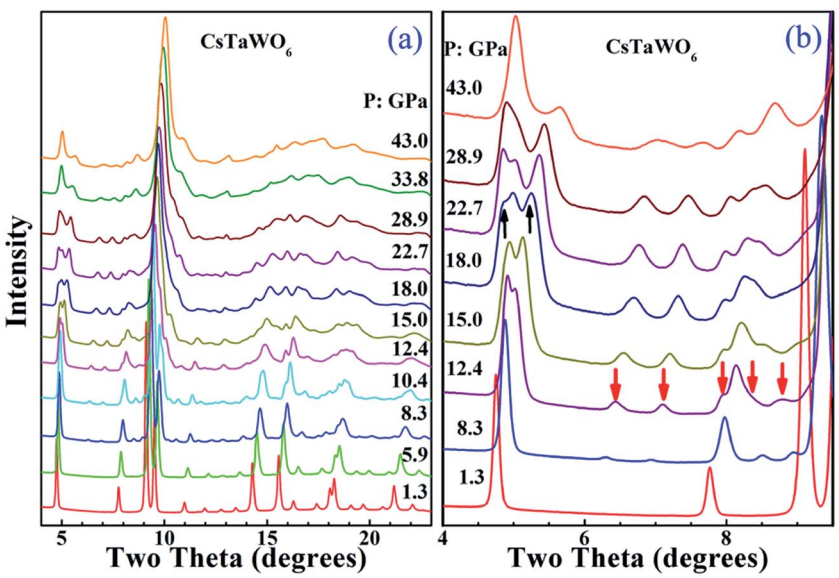

Fig. 2 XRD profiles of $CsTaWO_6$ at different pressures. The cubic structure becomes unstable at 8.3 GPa and an orthorhombic phase formed. A monoclinic high-pressure structure formed at pressure of 22.7 GPa.

cubic pyrochlore structure. With continued increases in the pressure, the split peaks separated gradually and split again at 18 GPa. At pressures higher than 33.8 GPa, two broad but well separated Bragg peaks were detected in the low 2θ region. The evolution of the XRD profiles suggests that $CsTaWO_6$ may have complicated phase transitions at high pressures.

Indexing of the Bragg peaks in the XRD patterns at pressure below 15.7 GPa indicated that the high-pressure phase is orthorhombic. Careful study of the XRD profiles suggested that the cubic-to-orthorhombic phase transition starts at even lower pressure of 5.9 GPa. Previous group-subgroup analysis[36] has revealed that pyrochlore structure ($Fd\bar{3}m$) with the loss of symmetry can be reduced to tetragonal, orthorhombic and monoclinic symmetries in the sequence: $Fd\bar{3}m \rightarrow I4_1/amd \rightarrow Imma \rightarrow Pnma \rightarrow P2_1/c$. Fortunately, an orthorhombic pyrochlore structure model with space group of *Pnma* was previously determined for the compound $CsMgInF_6$.[36,37] The XRD profiles of $CsTaWO_6$ at pressures below 15.7 GPa can be well refined using the orthorhombic structural model. Fig. 3b shows the fitting results of $CsTaWO_6$ at 10.4 GPa and the refined orthorhombic structure model at 5.9 GPa is illustrated in Table 1. The structural change from the cubic to the orthorhombic in $CsTaWO_6$ is a second-order phase transition, and there are no volume changes during the phase transition. The orthorhombic structure of the pyrochlore is formed through the distortion of the cubic structure without reconstruction. In the cubic structure model, the three crystallographic axes of the unit cell are equal, however, they become non-equivalent at high pressures resulting in the formation of an orthorhombic structure. The difference between the axes increases with the rising pressure. It is reasonable to believe that there is some difference between the axes in the starting cubic structure, which means that the

Table 1 Crystal structure of $CsTaWO_6$ at 5.9 GPa refined with space group of *Pnma* and lattice constants of $a = 7.224(2)$ Å, $b = 7.218(2)$ Å, $c = 10.167(2)$ Å, and fitting parameters of $R_p = 10.4$, $R_{wp} = 9.3$, $R_B = 4.3$, $R_F = 3.5$, $\chi^2 = 1.11$. The coordinates of all anions are not refined

Atom	Wyckoff	x/a	y/b	z/c	B	occ.
Cs	4c	0.5033(18)	$\frac{1}{4}$	0.3924(6)	0.1	1.0
Ta/W	4c	0.2303(8)	$\frac{1}{4}$	0.7602(7)	0.3	0.5/0.5
Ta/W	4b	0.0	0.0	$\frac{1}{2}$	0.3	0.5/0.5
O1	8d	0.3126	0.0549	0.8676	1.0	1.0
O2	8d	0.1991	0.4399	0.6220	1.0	1.0
O3	4c	0.4931	$\frac{1}{4}$	0.0710	1.0	1.0
O4	4c	0.0081	$\frac{1}{4}$	0.8134	1.0	1.0

starting phase may exhibit distortion from cubic symmetry. In fact, the cubic structure can be described as an equivalent tetragonal structure model perfectly, if half of the diagonal of one face of the cubic unit cell is selected as the a and b axes of the tetragonal unit cell. Such a tetragonal structure model with symmetry of $I4_1/amd$ has been built based on single crystal diffraction data for α-type pyrochlore $Sm_2Ti_2O_7$.[38] Similarly, a tetragonal structure model can be built for the β-type pyrochlore. Rietveld refinement with both cubic and tetragonal models shows no obvious difference between the fits. At ambient conditions, the lattice constant of a (or b) and c in the tetragonal model is 7.3258(7) Å and 10.333(2) Å, respectively, and the difference between a and $c/\sqrt{2}$ is 0.019 Å. The ~0.3% lattice mismatch suggests that the cubic structure has a tendency to be tetragonally distorted. With the increase of pressure, the difference between the unit cell parameters become more obvious, which results in a "real" phase transition. Fig. 4 shows the unit cell parameters of $CsTaWO_6$ refined with tetragonal structure model below 5.9 GPa and orthorhombic structure model between 8.3 GPa and 15 GPa. The c cell constant changes continuously during the phase transition, but the a and b cell constants separate gradually with increasing

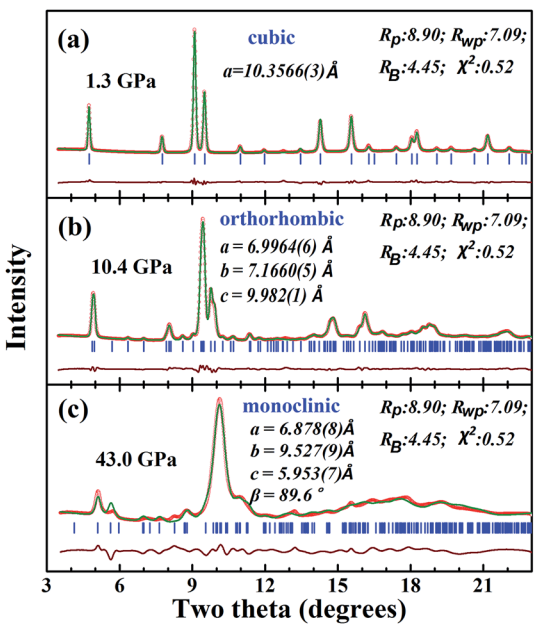

Fig. 3 The selected XRD diffraction patterns at (a) 1.3 GPa, (b) 10.4 GPa and (c) 43.0 GPa, which were refined with the cubic, orthorhombic and monoclinic structure models.

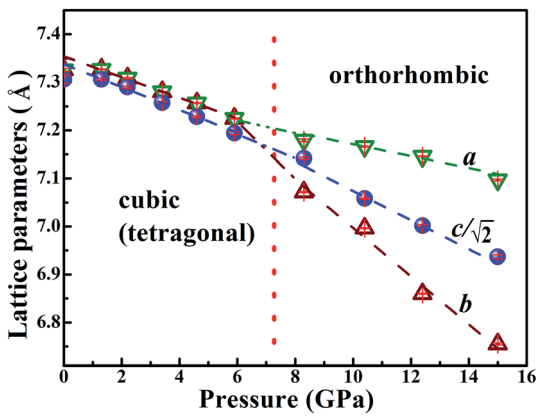

Fig. 4 Pressure dependence of the refined lattice parameters for the cubic and orthorhombic structures. The cubic structure, in fact, is tetragonally distorted. In order to make comparison, the cubic (tetragonal lattice) constants and c of the orthorhombic phase were divided by $\sqrt{2}$.

pressure. The difference between the *a* and *b* unit cell constants at 15 GPa is ~0.4 Å.

In the orthorhombic structure model (*Pnma*), there are only two allowed peaks ((011) and (101)) that are derived from the (111) peak of the cubic symmetry. Since the first Bragg peak splits into at least 3 peaks at pressures higher than 15 GPa, this suggests that the orthorhombic structure model is no longer correct at this pressure; it either loses symmetry elements and is reduced to an orthorhombic or monoclinic symmetry. Due to the broad and severe overlap of the individual Bragg peaks, the peaks in the high pressure XRD patterns cannot be well indexed with an orthorhombic or a monoclinic unit cell. They are probably a mixture of the orthorhombic and monoclinic high-pressure phases. A monoclinic structure model was built based on the known structure of $KCuCrF_6$.[39] The XRD patterns of $CsTaWO_6$ were refined with the mixture of the two phases at pressures between 18 GPa and 33.8 GPa, and with the single monoclinic phase at higher pressures. Although the patterns do not fit perfectly, the individual diffraction peak positions fit relatively well, which suggests that the monoclinic structure model is reasonable. The fitting of the XRD pattern at 43 GPa with the monoclinic structure model is shown in Fig. 3c, and the corresponding structure model is listed in Table 2. Since two of the 4 cation sites and all the anion sites are the general site 4e with variable coordinates (*x*, *y*, *z*), further refinement of these parameters in order to improve the fit is precluded. The unit cell parameters are correct through the whole-pattern fitting.

The structural evolution of $CsTaWO_6$ at high pressures is continuous and there is no volume collapse during the phase transitions. Fig. 5a and b show the schematic structures of the orthorhombic and monoclinic high-pressure phases. The orthorhombic high-pressure phase at pressures of 5–15 GPa has only slightly distorted from the initial phase, but the three crystalline axes are not equal. The structure has no major difference from the cubic (or tetragonal phase) viewing from [110] direction, but the *b*-axis became clearly shorter than the other two axes at high pressures. The structure of the monoclinic phase is clearly distorted from the cubic and orthorhombic phases. At least half of the $(TaW)O_6$ octahedra are severely distorted. As a result, the large channels surrounded by six octahedra, where Cs^+ cations are located, are obviously distorted. However, the $(TaW)O_6$ octahedral framework retains the same topology.

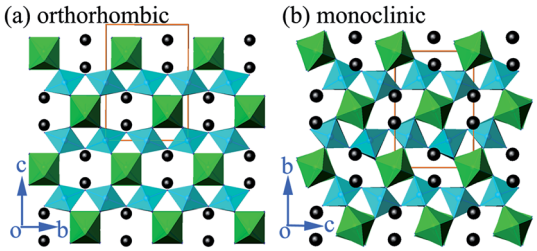

Fig. 5 The schematic crystal structures of the high-pressure phases of the β-type pyrochlores in symmetries of (a) orthorhombic; (b) monoclinic.

In both α- and β-type pyrochlores, the B_2O_6 octahedral framework is the same. As viewed along [110], there are two types of octahedral layers with different orientations, and the square bases of the octahedra between the two layers are nearly perpendicular. Structurally, the two octahedral layers are exactly equivalent. In the monoclinic structure, however, the cations in the center of the two layers are not the same as those in the cubic and orthorhombic phases, but rather form zigzag chains in the octahedral layers that are parallel to the *a*–*c* plane. Thus the pressure-induced phase transitions in the α- and β-type pyrochlores will have different mechanisms. In the β-type pyrochlores, pressure can only cause anisotropic compression through the rotation of the B_2O_6 octahedra and the framework retains the same topology. In α-type pyrochlores, the A-cations occupy the 16d site and resides in the voids of the B octahedral layers that are bonded to surrounding anions. The B cations are coordinated by six 48f oxygen, and the A-cation are surrounded by six 48f oxygen and two 8b oxygen with even shorter bonding length (~1.94 Å). At high pressure conditions, due to the shrinkage of the unit cell constant and tilting of the octahedra, the surrounding anions can have similar bonding environments for both A- and B-cations, and cations A and B can swap their sites forming cation anti-site defects. In the β-type pyrochlores, the larger A cation is on the 8b site. The distance between A and surrounding anions are longer than 3 Å and they are not chemically bonded. During the distortion of the octahedral framework, A-site cations still have enough space in the channel, and it is impossible to swap their sites with B-site cation in the center of the octahedral. Pressure-induced phase transitions in β-type pyrochlores thus have no atomic disordering of the cation and anion sublattices. The pressure-induced phase transitions in the α-type pyrochlore are more complicated.

The pressure dependence of the normalized unit cell volume (per molecule of $CsTaWO_6$) is plotted in Fig. 6. No volume collapse is expected in the *P*–*V* curve during the phase transitions from cubic (or tetragonal)-to-orthorhombic and from orthorhombic-to-monoclinic structures. Fitting with the 3rd order Birch–Murnaghan equation of state of the *P*–*V* curve below 18 GPa yields a bulk modulus of 46.8 GPa with $B' = 4$ as

Table 2 Crystal structure of $CsTaWO_6$ at 43.0 GPa refined with space group of $P2_1/c$ and lattice constants of $a = 6.878(8)$ Å, $b = 9.527(9)$ Å, $c = 5.953(7)$ Å, $\beta = 89.6°(1)$ and fitting parameters of $R_p = 10.4$, $R_{wp} = 11.3$, $R_B = 5.4$, $R_F = 3.0$, $\chi^2 = 1.57$. The coordinates of all anions are not refined

Atom	Wyckoff	*x*/*a*	*y*/*b*	*z*/*c*	B	occ.
Cs	4e	0.199(2)	0.859(1)	0.495(2)	0.5	1.0
Ta/W	4e	0.292(1)	0.3029(7)	0.8469(9)	0.8	0.5/0.5
Ta/W	2b	$\frac{1}{2}$	0.0	0.0	0.8	0.5/0.5
Ta/W	2a	0.0	0.0	0.0	0.8	0.5/0.5
O1	4e	0.9811	0.1663	0.8726	1.0	1.0
O2	4e	0.5068	0.8239	0.1041	1.0	1.0
O3	4e	0.2475	0.3290	0.0783	1.0	1.0
O4	4e	0.7531	0.0183	0.0799	1.0	1.0
O5	4e	0.0732	0.0851	0.2412	1.0	1.0
O6	4e	0.5560	0.5649	0.2499	1.0	1.0

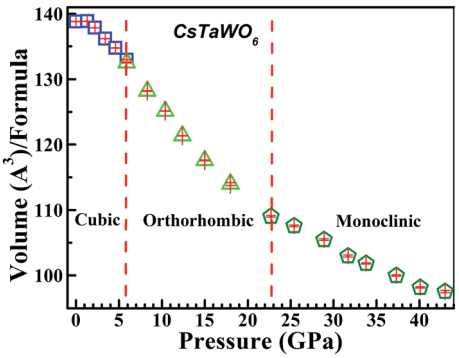

Fig. 6 The pressure dependence of the unit cell volume of $CsTaWO_6$, the continuity of the curve suggests a displacement phase transition in the pressure range. There is no obvious slope change from cubic to orthorhombic, but the slope change from orthorhombic to monoclinic indicates that the monoclinic high-pressure phase is difficult to be compressed.

the fixed zero pressure derivative for the starting cubic phase and orthorhombic phases. The monoclinic high-pressure phase is more difficult to compress and the bulk modulus fitted from the experimental data is 57.4 GPa ($B' = 4$). The bulk modulus of the β-type pyrochlores is obviously smaller than that of rare earth titanates and zirconates with normal pyrochlore structure (usually larger than 160 GPa).[6,7,9] This is because there are less cations in the β-type pyrochlores, resulting in more "free" space in the unit cell.

The Raman spectrum of $CsTaWO_6$ in a DAC was measured at pressure up to 40.4 GPa with methanol/ethanol pressure medium (Fig. 7). The measured Raman spectrum at low pressures is in good agreement with that previously reported.[40] Different from rare earth titanates, which have strong Raman signal,[6,7] the Raman modes of $CsTaWO_6$ are relatively weak and broad. This may be due to the presence of heavy elements Ta and W, and the disordering between them because they share the same crystallographic site. Group theory predicts[41] that the β-type pyrochlore has 6 Raman active modes $\Gamma = A_{1g} + E_g + 4T_{2g}$, where one T_{2g} is related to the Cs cation on the 8b site. Since the Ta^{5+} and W^{6+} occupy the same site, all the other modes related to O on the 48f site may split into two. It is difficult to index the observed Raman active modes from powder samples. The band with wavenumber below 70 cm^{-1} was difficult to be measured at ambient conditions. It shifted to higher wavenumbers at high pressures and is relatively sharp. It is the Cs-related translation mode (T_{2g}). The mode centered at ~130 cm^{-1} is the translation mode (T_{2g}) for Ta and W and obviously split at low pressures. The most intense bands between 530–750 cm^{-1} are caused by the vibration of the octahedral framework. As discussed in ref. 37, the two weak bands with wavenumber larger than 800 cm^{-1} are not second-order bands, but rather are due to the intrinsic vacancy in the B-site, which results in shorter ⟨B–O⟩ bonds. The bands thus have larger wavenumbers than the vibration modes from normal ⟨Ta–O⟩ and ⟨W–O⟩ bonds.

The phase transition from the cubic (or tetragonal) to the orthorhombic phase is difficult to be identified from the measured Raman spectra. The change of some Raman active modes in the spectra above 15.7 GPa is distinct. The mode centered at ~120 cm^{-1} at ambient conditions has a large shift to higher wavenumbers, however, the strongest bands at ~700 cm^{-1} and the band at ~980 cm^{-1} shift to lower wave numbers anomalously. The detailed pressure dependence of the main Raman active modes is shown in Fig. 7b. The different pressure dependences of the Raman modes suggest that some bonds may be expanded during the orthorhombic-to-monoclinic phase transition due to the severe distortion of the B_2O_6 octahedral framework. After the phase transition, the pressure-dependences of all the Raman active modes follow the general

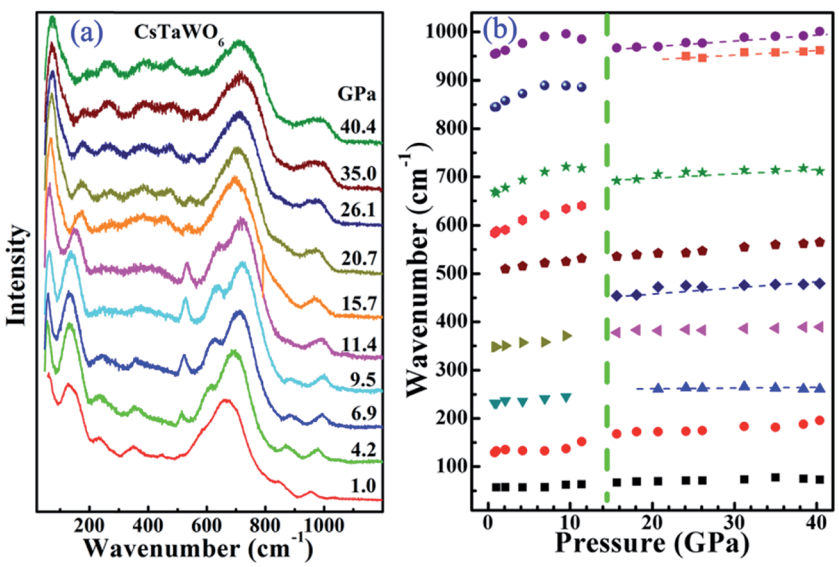

Fig. 7 Raman spectra of $CsTaWO_6$ at high pressures. The pressure-induced phase transition from the cubic to the orthorhombic phase (below 15.7 GPa) has no distinct changes in the spectrum, but the transition from orthorhombic to monoclinic corresponds a distinct change in the spectrum, and some Raman modes (centered at ~680 cm^{-1} and 950 cm^{-1}) shift to lower wavenumbers.

rule—increasing the wavenumber because of the compression of the bands. Several new modes appeared in the 200–600 cm^{-1} wavenumber range in the monoclinic phase, which suggests that the high-pressure phase has a lower symmetry and the anions around the Ta- or W-cations have more degree of freedom.

Superconductivity was found in a group of alkaline osmium oxides (AOs_2O_6) with the isostructural β-type pyrochlore structure before.[25–30] The discovery caused great research interests in the field because they are copper-free superconductors, although the critical transition temperature is low. The pressure effect on the superconductivity was also investigated. Both resistivity and magnetization measurements at high pressures[42] suggested that the critical transition temperature increases with the increase of pressure and then drops at higher pressures. Our structural studies suggest that similar pressure-induced phase transition may occur in the isostructural AOs_2O_6 pyrochlores and the critical superconducting temperature may relate to the structure changes at high pressures.

IV. Conclusions

In summary, pressure-induced structural transitions in $CsTaWO_6$ with the β-type pyrochlore structure were studied by XRD and Raman scattering measurement and compared with α-type pyrochlores. The structure transformations from the cubic (or tetragonal) to an orthorhombic high-pressure phase at 5.9 GPa and further to a monoclinic structure at 15.7 GPa are confirmed by XRD and Raman scattering measurements. There is no volume collapse during the phase transitions. Different from the α-type pyrochlore, the Cs^+ cation is not bonded with neighboring anions and does not change the occupancy with Ta^{5+} and W^{6+} on the B-site in all the high-pressure structures, although the octahedral framework in the β-type pyrochlore $CsTaWO_6$ is severely distorted at high pressures. The pressure-induced structural changes in normal α-type pyrochlore oxides are more complicated.

Acknowledgements

This work is supported by Department of Energy (DOE) Stewardship Science Academic Alliances program, National Nuclear Security Administration of the U.S. Department of Energy under award number DE-NA0001977. The XRD measurement was performed at beam 16-BMD, HPCAT, Advanced Photon Source, Argonne National Laboratory. HPCAT operations are supported by DOE-NNSA under Award No. DE-NA0001974 and DOE-BES under Award No. DE-FG02-99ER45775, with partial instrumentation funding by NSF. The Advanced Photon Source is a U.S. Department of Energy (DOE) Office of Science User Facility operated for the DOE Office of Science by Argonne National Laboratory under Contract No. DE-AC02-06CH11357.

References

1 M. A. Subramanian, G. Aravamudan and G. V. Subba Rao, *Prog. Solid State Chem.*, 1983, **15**, 55–143.
2 J. Isasi, M. L. Lopez, M. L. Veiga, E. Ruizhutzky and C. Pico, *J. Solid State Chem.*, 1995, **116**, 290–295.
3 J. B. Thomson, A. R. Armstrong and P. G. Bruce, *J. Solid State Chem.*, 1999, **148**, 56–62.
4 J. Wang, A. Nakamura and M. Takeda, *Solid State Ionics*, 2003, **164**, 185–191.
5 D. Errandonea, R. S. Kumar, S. N. Achary, O. Gomis, F. J. Manjon and R. Shukla, *J. Appl. Phys.*, 2012, **111**, 053519.
6 F. X. Zhang, B. Manoun, S. K. Saxena and C. S. Zha, *Appl. Phys. Lett.*, 2005, **86**, 181906.
7 F. X. Zhang, J. W. Wang, J. Lian, M. K. Lang, U. Becker and R. C. Ewing, *Phys. Rev. Lett.*, 2008, **100**, 045503.
8 F. X. Zhang, M. Lang, R. C. Ewing and Z. X. Liu, *Phys. Rev. Lett.*, 2010, **105**, 015503.
9 F. X. Zhang, M. Lang and R. C. Ewing, *Appl. Phys. Lett.*, 2015, **106**, 191902.
10 J. Lian, L. M. Wang, J. Chen, K. Sun, R. C. Ewing, J. M. Farmer and L. A. Boatner, *Acta Mater.*, 2003, **51**, 1493–1502.
11 B. D. Begg, N. J. Hess, D. E. McCready, S. Thevuthasan and W. J. Weber, *J. Nucl. Mater.*, 2001, **289**, 188–193.
12 J. Lian, X. T. Zu, K. V. G. Kutty, J. Chen, L. M. Wang and R. C. Ewing, *Phys. Rev. B*, 2002, **66**, 054108.
13 S. X. Wang, B. D. Begg, L. M. Wang, R. C. Ewing, W. J. Weber and K. V. G. Kutty, *J. Mater. Res.*, 1999, **14**, 4470–4473.
14 H. L. Tuller, *Solid State Ionics*, 1992, **52**, 135–146.
15 B. J. Wuensch, K. W. Eberman, C. Heremans, E. M. Ku, P. Onnerud, E. M. E. Yeo, S. M. Haile, J. K. Stalick and J. D. Jorgensen, *Solid State Ionics*, 2000, **129**, 111–133.
16 R. C. Ewing, W. Weber and J. Lian, *J. Appl. Phys.*, 2004, **95**, 5949–5971.
17 G. Catillon and A. Chartier, *J. Appl. Phys.*, 2014, **116**, 193502.
18 P. M. van Dijk, K. J. deVries and A. J. Burggraaf, *Solid State Ionics*, 1983, **9/10**, 913–919.
19 J. Lian, L. M. Wang, R. G. Harie, K. B. Helean and R. C. Ewing, *Nucl. Instrum. Methods Phys. Res., Sect. B*, 2004, **218**, 236–243.
20 S. Uma, J. Singh and V. Thakral, *Inorg.Chem.*, 2009, **48**, 11624–11630.
21 L. H. Bastsle, D. Huys and J. Inorg, *Nucl. Chem.*, 1968, **30**, 639–649.
22 T. Moller, A. Clearfield and R. Harjula, *Chem. Mater.*, 2001, **13**, 4767–4772.
23 S. Zouad, J. Jeanjean, C. Loos-Neckovic, M. Federoff and Y. Piffard, *J. Radioanal. Nucl. Chem.*, 1994, **182**, 193–204.
24 C. Konecny and V. Kourim, *Radiochem. Radioanal. Lett.*, 1968, **2**, 47.
25 J. Yamaura, S. Yonezawa, Y. Muraoka and Z. Hiroi, *J. Solid State Chem.*, 2006, **179**, 336–340.
26 S. Yonezawa, Y. Muraoku, Y. Matsushita and Z. Hiroi, *J. Phys.: Condens. Matter*, 2004, **16**, L9–L12.
27 M. Hanawa, Y. Muraoka, T. Tayama, T. Sakakibara, J. Yamaura and Z. Hiroi, *Phys. Rev. Lett.*, 2001, **87**, 187001.
28 S. Yonezawa, Y. Muraoka, Y. Matsushita and Z. Hiroi, *J. Phys.: Condens. Matter*, 2004, **16**, L9–L12.
29 S. Yonezawa, Y. Muraoka and Z. Hiroi, *J. Phys. Soc. Jpn.*, 2004, **73**, 1655–1656.

30 S. Yonezawa, Y. Muraoka, Y. Matsushita and Z. Hiroi, *J. Phys. Soc. Jpn.*, 2004, **73**, 819–821.
31 T. Kar and R. N. P. Choudhary, *Mater. Sci. Eng., B*, 2002, **90**, 224–233.
32 K. Miyoshi, Y. Takaichi and Y. Takamatsu, *J. Phys. Soc. Jpn.*, 2008, **77**, 043704.
33 H. K. Mao, J. Xu and P. M. Bell, *J. Geophys. Res.*, 1986, **91**, 4673–4676.
34 A. P. Hammersley, *Fit 2d*, ESRF, Grenoble, France, 1998.
35 J. Rodriguez-Carvajal, Recent Developments of the Program FULLPROF, in Commission on Powder Diffraction (IUCr), *Newsletter*, 2001, **26**, 12–19.
36 A. Grzechnik, W. Morgenroth and K. Friese, *J. Solid State Chem.*, 2009, **182**, 1792–1797.
37 M. S. Molokeev, E. V. Bogdanov, S. V. Misyul, A. Tressaud and I. N. Flerov, *J. Solid State Chem.*, 2013, **200**, 157–164.
38 M. E. Rabanal, A. Varez, U. Amador, E. A. Y. Dompablo and F. Garcia-Alvarado, *J. Mater. Process. Technol.*, 1999, **93**, 529–533.
39 D. Kissel and R. Hoppe, *Z. Anorg. Allg. Chem.*, 1988, **557**, 161–170.
40 M. Maczka, A. V. Knyazev, A. Majchrowski, J. Hanuza and S. Kojima, *J. Phys.: Condens. Matter*, 2012, **24**, 195902.
41 E. Kroumova, M. I. Aroyo, J. M. Perez-Mato, A. Kirov, C. Capillas, S. Ivantchev and H. Wondratschek, *Phase Transitions*, 2003, **76**, 155–170.
42 T. Muramatsu, N. Takeshita, C. Terakura, H. Takagi, Y. Tokura, S. Yonzawa, Y. Muraoka and Z. Hiroi, *Phys. B*, 2006, **378–380**, 882–883.